Numerical Simulations of Sand Elements Based on Constant-Volume versus True-Undrained Data from Cyclic Direct Simple Shear Tests

Catherine T. Nguyen[1]; Wing Shun Kwan, Ph.D., P.E., M.ASCE[2]; and Cesar Leal[3]

[1]Research Associate, Dept. of Civil Engineering, California State Univ., Los Angeles.
Email: cnguye223@calstatela.edu
[2]Associate Professor, Dept. of Civil Engineering, California State Univ., Los Angeles.
Email: wkwan4@calstatela.edu
[3]Graduate Research Assistant, Dept. of Civil Engineering, California State Univ., Los Angeles.
Email: cleal5@calstatela.edu

Downloaded from ascelibrary.org by California State University, Los Angeles on 03/07/25. Copyright ASCE. For personal use only; all rights reserved.

ABSTRACT

Numerical simulation of liquefiable soil under cyclic undrained loading is essential for predicting earthquake-induced deformation of geotechnical structures in liquefaction hazard evaluation. Successful simulation of soil response requires constitutive models that can reasonably predict soil behavior under dynamic loading. Many advanced constitutive models have been developed for soil liquefaction hazard evaluation in the past four decades. These advanced models are built on plasticity theories with different modifications and assumptions. Nevertheless, the core part of all models was mainly developed based on observations from constant-volume (CV) cyclic direct simple shear (DSS) tests. While CV tests are standardized in the widely recognized ASTM D8296-19, true-undrained (TU) cyclic DSS tests wherein pore water pressure (PWP) is directly measured have also been performed in academic research. CV and TU cyclic DSS data were successfully generated at California State University, Los Angeles (Cal State LA), from the same apparatus. In this paper, the PM4Sand plasticity model is calibrated using CV and TU data. The performance of CV- and TU-calibrated models is cross-compared with TU and CV data, respectively. While results suggest trends in liquefaction capacity predictions, further data is required for comprehensive validation. The outcomes of this paper also provide insight into the calibration of PM4Sand over a range of relative densities and loading conditions.

INTRODUCTION

The advent of soil constitutive models has been critical in performing robust evaluations of liquefaction hazard, allowing for prediction of soil behavior under dynamic loading. These models describe the stress-strain response of soils using theories of solid mechanics and are typically calibrated on extensive experimental datasets and case histories to achieve reasonable performance across a broad range of conditions (Ziotopoulou et al. 2018).

Dynamic laboratory soil tests such as cyclic DSS and triaxial tests are instrumental in the calibration of such models. The widely recognized ASTM D8296-19 provides provisions for conducting undrained cyclic DSS tests (ASTM 2019). Under ASTM D8296-19, undrained conditions are implemented via active or passive height control of the top plate of the shear apparatus to keep the sample volume constant throughout shear. The resulting sample stress response has been shown to correlate well with PWP generation in TU tests (Finn and Vaid 1977, Dyvik et al. 1987). This allows for relatively quick, equivalent-undrained testing on dry specimens.

© ASCE

Downloaded from ascelibrary.org by California State University, Los Angeles on 03/07/25. Copyright ASCE. For personal use only; all rights reserved.

Despite the practical advantages of CV tests, their prevalence in experimental calibration datasets raises questions about their equivalence to TU tests. There is limited literature comparing CV and TU methods; Finn and Vaid (1977) found that PWP responses from CV and TU cyclic DSS tests on Ottawa sand were practically equivalent, and that the CV tests tended to underpredict liquefaction capacity compared to TU tests. Dyvik et al. (1987) conducted CV and TU monotonic DSS tests on normally consolidated clay and found similar PWP generation and stress-strain responses. Zhang and Rothenburg (2020) were able to discern differences in numerical modelling of CV vs. TU conditions under monotonic loading using discrete element modelling (DEM). They concluded that conditions conducive to rapid PWP dissipation, such as loose, coarse sands are well-modelled by CV approaches, but fluid-coupling, which is more representative of TU conditions, is more appropriate for denser configurations. Similar conclusions were drawn from a DEM study by Hanley et al. (2013) that conducted monotonic triaxial simulations and found that very dense materials may violate CV assumptions because sample stresses may become so high that water can no longer be considered incompressible.

The insights of these studies are valuable, but mainly focus on the differences in the mechanical behavior observed between the two test methods. To the authors' knowledge, there has been limited exploration into the impacts of CV vs. TU data-calibrated constitutive models, specifically in the context of predicting liquefaction. The output of a constitutive model is highly dependent on the data it is calibrated on. Therefore, it is important to understand the implications of calibrating to experimental results derived using different methods, especially when the model will be used to make critical predictions as is the case with liquefaction hazard evaluations. This study aims to provide preliminary insights into the effects of CV vs. TU test-based calibration datasets on predicted liquefaction capacity using the PM4Sand plasticity model, Version 3.1 (Boulanger and Ziotopoulou 2017) implemented in Version 8.0 of FLAC, a two-dimensional explicit finite difference numerical modelling software commonly used in geotechnical engineering practice (Itasca 2016).

EXPERIMENTAL DATA

The data for this study is sourced from two experimental programs and consists of tests performed on Ottawa sand (C_u = 1, C_c = 1.7, D_{60} = 0.39 mm, D_{30} = 0.3 mm, D_{10} = 0.23 mm, USCS = SP, γ_{min} = 14.74 kN/m^3, and γ_{max} = 17.22 kN/m^3), a poorly graded clean sand with rounded grains that is commonly used in liquefaction research (El Ghoraiby et al., 2017). Testing conditions are summarized in Tables 1 and 2 for Datasets 1 and 2, respectively. D_r corresponds to post-K_0 consolidation, pre-shear relative densities. The number of uniform cycles until failure (N_f) is presented based on the excess PWP ratio (r_u = 0.95) liquefaction triggering criteria.

Table 1. Testing conditions for Dataset 1 tests.

Test ID	Type	Method	CSR	D_r	σ'_{v0} (kPa)	N_f, r_u = 0.95
D1_1	Stress-controlled Cyclic DSS	CV	0.125	61%	198	30.6
D1_2	Stress-controlled Cyclic DSS	CV	0.16	50%	197	8.1
D1_3	Stress-controlled Cyclic DSS	CV	0.16	69%	205	6.1
D1_4	Stress-controlled Cyclic DSS	CV	0.21	52%	200	3.1

All tests were performed at Cal State LA on a Confined Multi-Directional Dynamic Simple Shear (CMDSS) device equipped with a six-axis load cell and three Linear Variable Differential

© ASCE

Downloaded from ascelibrary.org by California State University, Los Angeles on 03/07/25. Copyright ASCE. For personal use only; all rights reserved.

Transformers (LVDTs) measuring displacement along the X, Y, and Z axes and allowing for active height control for CV testing (Figure 1). The CMDSS device also features a dedicated pressure-controller for back-pressure saturation and a PWP transducer, making TU testing possible. More detailed information on the device is documented in Kwan et al. (2025).

Table 2. Testing conditions for Dataset 2 tests.

Test ID	Type	Method	CSR	D_r	σ'_{v0} (kPa)	N_f, r_u=0.95
D2_1	Stress-controlled Cyclic DSS	TU	0.31	61%	72	2.1
D2_2	Stress-controlled Cyclic DSS	CV	0.26	55%	79	1.1

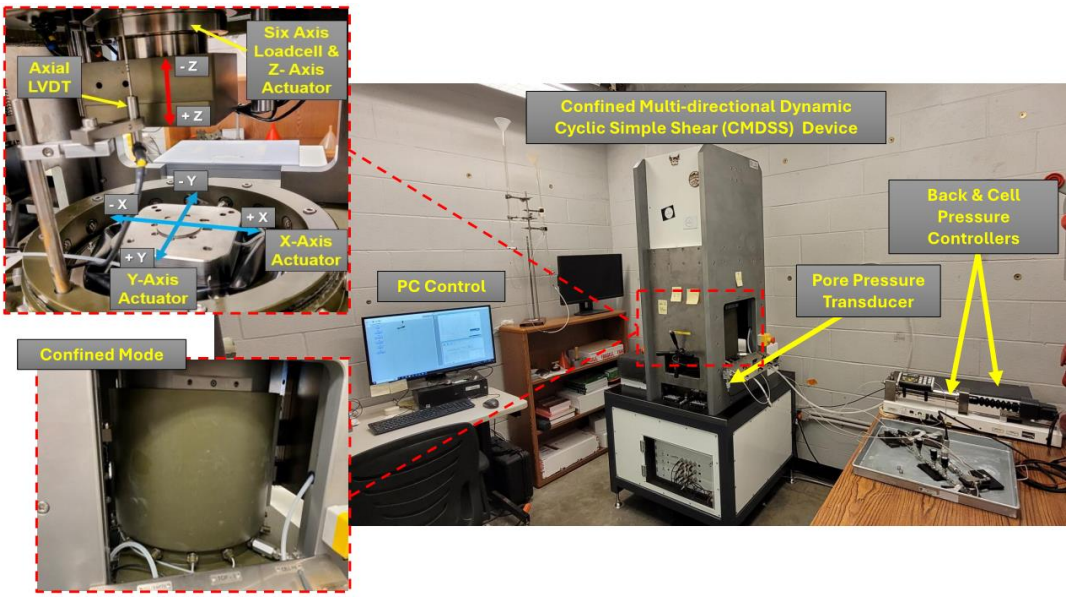


Figure 1. Experimental setup.

Samples were reconstituted via dry pluviation to a nominal diameter of 65-mm for CV samples and 99-mm for TU samples, with pre-shear heights ranging from 18-22 mm. The TU specimen was prepared in a larger mold to reduce impacts of localized boundary effects on PWP generation. K_0 conditions were achieved using a reinforced membrane confined by 1.1-mm thick, Teflon-coated rings stacked to the height of the sample, allowing for natural rotation of principal stresses and constant sample diameter throughout shear.

CALIBRATION PROCEDURE

PM4Sand contains 24 input parameters; at minimum, inputs for the following three parameters are required for calibration: relative density D_r, shear modulus coefficient G_o, and contraction rate parameter h_{po}. D_r is the primary variable controlling stress-strain response and dilatancy, G_o primarily controls small-strain stiffness, and h_{po} primarily controls volumetric contraction rates in the plastic regime. Default values are provided for the 21 additional secondary parameters and can be adjusted if soil-specific data are available (Boulanger and Ziotopoulou 2017). A publicly available calibration driver by Boulanger and Ziotopoulou written in FLAC's internal FISH language was used and modified to automate parts of the calibration

© ASCE

process. It should be noted that although the driver implements TU boundary conditions, it was also used to calibrate PM4Sand to CV data. This reflects a practical approach commonly used by engineers who rely on accessible tools but may not have the numerical modelling expertise to modify boundary conditions for their specific datasets.

An outline of the calibrations and simulations performed is presented in Figure 2. Calibrated model performances are evaluated by simulating and comparing to experimental results conducted under high-liquefaction potential loading conditions, i.e. high CSR > 0.20. CV calibrations were used to simulate a TU test, and a TU calibration was used to simulate two CV tests. Calibration procedures are further discussed below, and a summary of the final calibration parameters is presented at the end of the section.

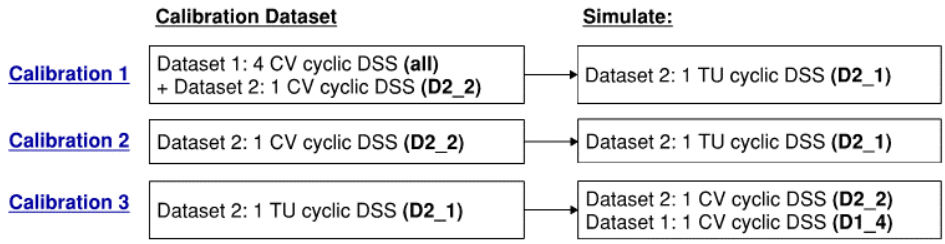


Figure 2. Summary of calibrations and simulations performed in this study.

Calibration 1: CV cyclic DSS capacity curve

Calibration 1 prioritized reproduction of the capacity curve (CSR vs. N_f, r_u = 0.95) fitted to Dataset 1 and the CV cyclic DSS test from Dataset 2 (Test D2_2). Although Dataset 1 was performed at σ'_{v0} = 200 kPa compared to 79 kPa for Test D2_2, D2_2 was incorporated to utilize as much available test data as possible; additionally, Test D2_2 had the closest CSR to the target simulation conditions and would help constrain the capacity curve at high CSR-low cycle counts. Test D2_2's CSR was adjusted by the overburden factor K_σ recommended from proceedings of the 1996 and 1998 NCEER workshops on soil liquefaction resistance (Youd et al., 2001).

$$K_\sigma = \left(\frac{\sigma'_{v0}}{p_a}\right)^{f-1} \tag{1}$$

$$CSR_{\sigma'_{v0}} = K_\sigma CSR_{pa} \tag{2}$$

where p_a is atmospheric pressure taken as 101.3 kPa, and f is a function of site conditions including D_r, stress history, and aging. Youd et al. recommend f = 0.7-0.8 for D_r of 40-60%. For simplicity, f was taken as the upper limit (0.8) for the proceeding calculations, given the majority of Dataset 1 and Test D2_2 was performed on samples with D_r 50-60%, except for Test D1_3 performed at Dr = 69%. Therefore, Test D2_2's adjusted CSR is calculated as follows:

$$K_{\sigma'_{v0}=79\ kPa} = \left(\frac{79\ kPa}{101.3\ kPa}\right)^{0.8-1} = 1.05$$

$$K_{\sigma'_{v0}=200\ kPa} = \left(\frac{200\ kPa}{101.3\ kPa}\right)^{0.8-1} = 0.87$$

© ASCE

Downloaded from ascelibrary.org by California State University, Los Angeles on 03/07/25. Copyright ASCE. For personal use only; all rights reserved.

$$CSR_{\sigma'_{v0}=200\ kPa} = CSR_{\sigma'_{v0}=79\ kPa} \frac{K_{\sigma'_{v0}=79\ kPa}}{K_{\sigma'_{v0}=200\ kPa}} = 0.26 \times \frac{1.05}{0.87} = 0.31$$

A capacity curve was then fit to the combined dataset to a power function of form CSR = $a \cdot N^{-b}$ using MATLAB's Curve Fitting toolbox (MathWorks 2024).

Model calibration consisted of single-element simulations of each test comprising the capacity curve, and iterative adjustment of model parameters until the simulated N_f matched predicted N_f values from the capacity curve. D_r was input as reported in Tables 1-2. Shear wave velocity (V_s) measurements were not taken during the experiments, so there was little information to constrain G_o. The default calibration for G_o, which incorporates Andrus and Stokoe's (2000) V_s correlation with corrected SPT blow count $(N_1)_{60}$, was used accordingly. $(N_1)_{60}$ was derived from the input D_r via the following expression by Idriss and Boulanger (2008) for clean sands:

$$(N_1)_{60} = 46 \cdot D_r^2 \tag{3}$$

Per recommendation by Boulanger and Ziotopoulou (2017), the third primary parameter h_{po} was calibrated last, as it is sensitive to the values of other parameters. In most studies documenting PM4Sand calibrations, such as in Lingwall (2017), Ziotopoulou (2018), and Anthi and Gerolymos (2019), h_{po} is calibrated as a single constant. These studies calibrate PM4Sand to capacity curves in CSR vs. N_f space consisting of tests at the same, or very similar D_r. While the dataset is in the medium-dense to dense range (D_r=50-69%), there is considerable variation in D_r. Consequently, attempting to reproduce the capacity curve based on a single value for h_{po} proved difficult. Plotting N_f resulting from various calibrated h_{po} shows that the tests exhibit varying sensitivities to h_{po}, possibly related to the varying D_r (Figure 3a). In particular, modelled liquefaction capacities for D1_1 and D1_3 showed higher sensitivities to h_{po} compared to the other tests. Plotting CSR vs. D_r of the tests suggests that for higher D_r and lower CSR, modelled liquefaction capacity and therefore sensitivity to calibrated h_{po} increases. Furthermore, visually, the different N_f sensitivities to h_{po} can be more easily clustered based on D_r than CSR, suggesting that the effect of D_r is greater than CSR (Figure 3b). This observation is further supported by Kruskal-Wallis tests using a binary classification of N_f sensitivity to h_{po} (D1_1 and D1_3 labelled as high and D1_2, D1_4, and D2_2 labelled as low). The tests show a smaller p-value for groupings based on D_r ($p = 0.08$) compared to CSR ($p = 0.13$), indicating that D_r is more strongly associated with N_f sensitivity to h_{po}. For a capacity curve generated from a dataset with considerably varying D_r, calibrating h_{po} as a function of D_r can allow modelers to achieve better calibration fits.

Luna et al. (2024) proposed a framework for developing a three-dimensional liquefaction triggering surface relating CSR, D_r, and N_f. In the study, a PM4Sand calibration was demonstrated on a cross-section of the surface corresponding to a capacity curve in CSR vs. D_r space at constant N_f. h_{po} was calibrated as a function of D_r, rather than as a constant, in the form $\log(h_{po}) = a \cdot D_r^2 + b \cdot D_r + c$ where a, b, and c are calibration constants. Results from plotting $\log(h_{po})$ vs. D_r, where h_{po} values are those resulting in the N_f predicted by the fitted capacity curves, are shown in Figure 4a. The calibration drivers provided by Boulanger and Ziotopoulou (2017) count cycles in increments of 0.5; therefore, where the same N_f was predicted for various h_{po}, the h_{po} from the first occurrence of the desired N_f was selected. The scatter indicated a negative correlation between h_{po} and D_r ($R = -0.65$). Several curve fits of the scatter were trialed,

Downloaded from ascelibrary.org by California State University, Los Angeles on 03/07/25. Copyright ASCE. For personal use only; all rights reserved.

© ASCE

Downloaded from ascelibrary.org by California State University, Los Angeles on 03/07/25. Copyright ASCE. For personal use only; all rights reserved.

including quadratic (R^2 = 0.59) and linear (R^2 = 0.42). While Luna et al. used a quadratic fit, MATLAB's Curve Fitting toolbox consistently fitted a concave-up quadratic function to the scatter, resulting in h_{po} both increasing and decreasing within the D_r range of interest. In contrast, the fitted quadratic function to h_{po} vs. D_r in Luna et al.'s study is concave down with h_{po} monotonically decreasing with increasing D_r for D_r = 20-80%. This is physically consistent with denser soils having less tendency to exhibit contractive behavior. To preserve this monotonically decreasing trend, h_{po} was instead calibrated to a linear function of the form $\log(h_{po}) = a \cdot D_r + b$, shown in Figure 4a. The log transformation was applied to avoid negative values of h_{po}. All secondary parameters were kept at their default values. The fitted experimental vs. calibrated capacity curves are presented in Figure 4b.

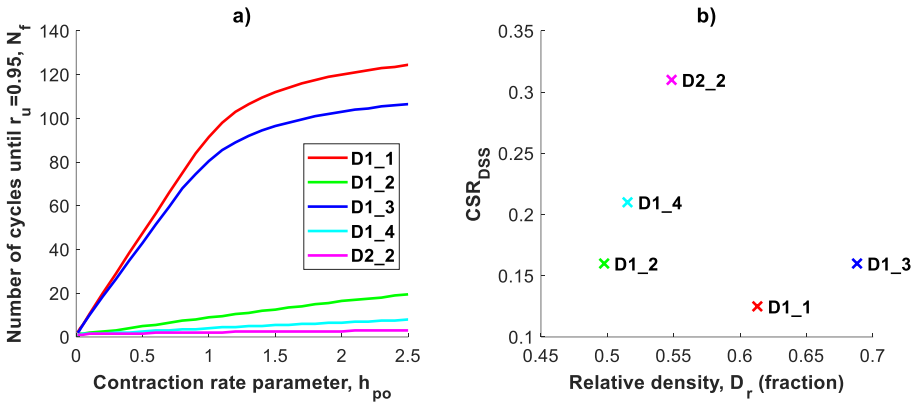


Figure 3. a) Sensitivity of liquefaction capacity (cycles until failure) to h_{po}. b) CSR vs. D_r for simulations performed under test conditions for Dataset 1 tests and Test D2_2.

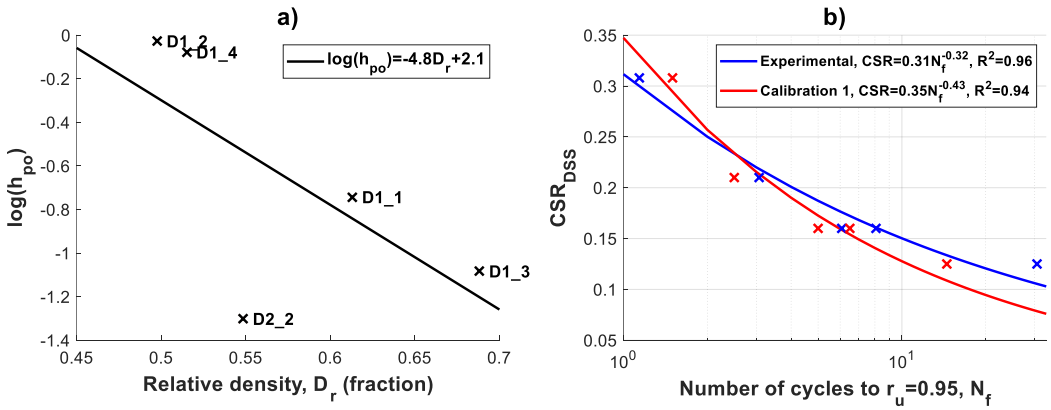


Figure 4. a) h_{po} calibrated as a function of D_r. b) Experimental vs. calibrated capacity curves. The experimental capacity curve was derived from Dataset 1 tests and overburden-corrected Test D2_2.

Calibrations 2 & 3: Single CV cyclic DSS test & single TU cyclic DSS test

Recognizing that the target simulation conditions for Calibration 1 are in the instability region of the capacity curve, wherein liquefaction resistance changes rapidly with minor

© ASCE

Downloaded from ascelibrary.org by California State University, Los Angeles on 03/07/25. Copyright ASCE. For personal use only; all rights reserved.

variations in CSR, the performance of a calibration based on a single test performed under similar conditions was of particular interest. This is the purpose of Calibration 2. Although it is generally good practice to calibrate to a capacity curve, the need to make accurate predictions in the instable region may require an alternate approach. Many curve-fitting algorithms use least-squares regression, which treats all errors equally. Consequently, fitting a "general purpose" capacity curve covering a broad range of conditions could compromise model performance in the instability region, as least-squares regression does not prioritize minimizing error in any specific region. For the TU cyclic DSS calibration, which is the purpose of Calibration 3, calibration to a single test is also necessitated by limited data as the dataset contains only one TU cyclic DSS test, Test D2_1.

As in Calibration 1, calibrations were performed on single elements simulated under target test conditions. The calibration procedure for a single test involved the same D_r and G_o input processes as in Calibration 1. Unlike in Calibration 1, h_{po} was calibrated as a single constant and iteratively adjusted until the simulated N_f matched the experimental N_f. Due to coarse granularity in cycle counts from the calibration driver, h_{po} was selected at first occurrence of the desired N_f. All secondary parameters were kept at their default values.

Table 3. Results of Calibrations 2 and 3.

Calibration #	Calibrated Test	N_f, experimental	N_f, simulated	% difference	Bias
2 (CV)	D2_2 (CV)	1.1	1	-9.1%	-0.1
3 (TU)	D2_1 (TU)	2.1	2	-4.8%	-0.1

Table 4. Resulting calibration parameters. Secondary parameters were not adjusted.

Calibration #	Calibrated Test	D_r	G_o	h_{po}
1	Dataset 1 + D2_2	User input	Default with Equation 3	$\log(h_{po}) = -4.8D_r+2.1$
2	D2_2			0.11
3	D2_1			0.01

SIMULATION RESULTS

A comparison of simulated vs. experimental N_f is presented in Table 5. Simulated vs. experimental cyclic responses (stress path, stress-strain, and PWP generation) are presented in Figures 5, 6, and 7. Mean errors between experimental and simulated excess PWP ratio are presented in Table 6 as an additional metric to assess model bias. Mean errors are calculated for an overall range of $0 < N < N_f$ cycles, where N_f is the lower of the experimental or simulated values, and for an early-stage range of $0 < N < 0.5$ cycles.

Table 5. Comparison between simulated and experimental N_f.

Calibration #	Simulated Test	CSR	N_f, experimental	N_f, simulated	% difference	Bias
1 (CV)	D2_1 (TU)	0.31	2.1	2	-4.7%	-0.1
2 (CV)	D2_1 (TU)	0.31	2.1	1	-52%	-1.1
3 (TU)	D1_4 (CV)	0.21	3.1	1.5	-52%	-1.6
3 (TU)	D2_2 (CV)	0.26	1.1	1.5	+36%	+0.4

© ASCE

Downloaded from ascelibrary.org by California State University, Los Angeles on 03/07/25. Copyright ASCE. For personal use only; all rights reserved.

TU cyclic DSS test predictions (Calibrations 1 & 2)

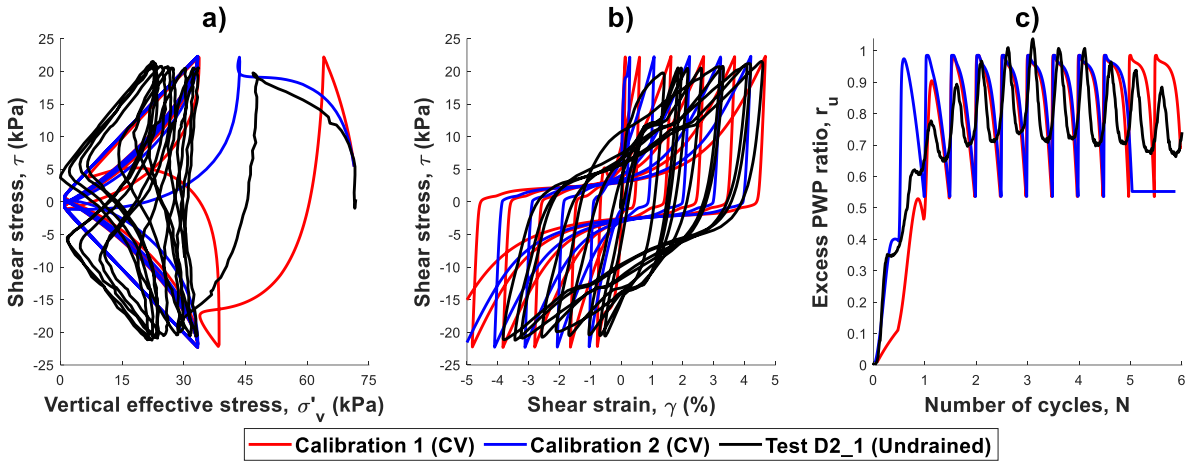


Figure 5. CV-calibrated simulations of TU cyclic DSS loading response (Test D2_1, D_r 61%, CSR 0.31, σ'_{v0} = 72 kPa). a) Stress path, b) Stress-strain curve, c) PWP generation.

CV cyclic DSS test predictions (Calibration 3)

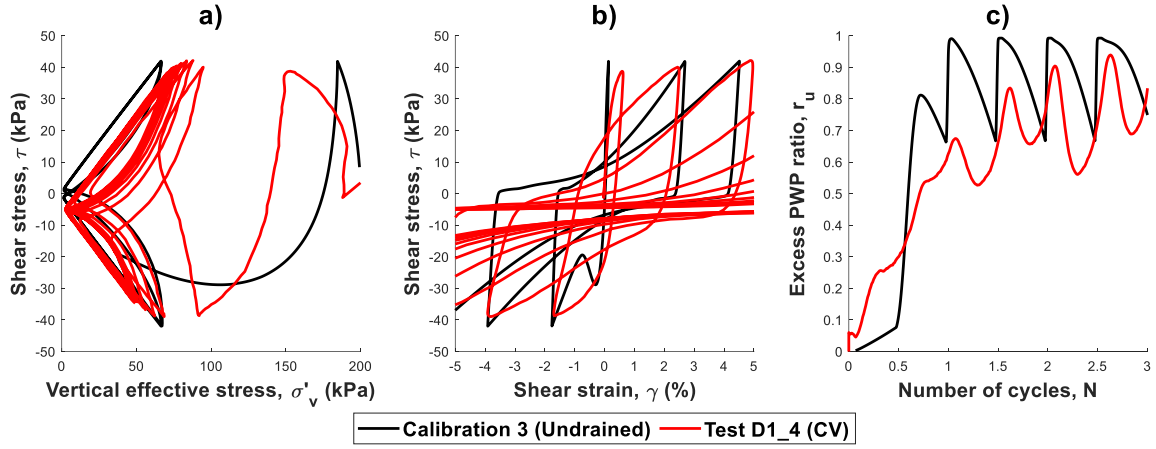


Figure 6. TU-calibrated simulations of CV cyclic loading response (Test D1_4, D_r 52%, CSR 0.21, σ'_{v0} = 200 kPa). a) Stress path, b) Stress-strain curve, c) PWP generation.

Table 6. Mean errors between experimental and simulated excess PWP ratio.

Calibration #	Simulated Test	Selected N_f	Overall mean error, Excess PWP ratio for $0 < N < N_f$	Early-stage mean error, Excess PWP ratio for $0 < N < 0.5$
1 (CV)	D2_1 (TU)	2	0.01	0.22
2 (CV)	D2_1 (TU)	1	-0.19	-0.01
3 (TU)	D1_4 (CV)	1.5	-0.21	0.18
3 (TU)	D2_2 (CV)	1.1	0.08	0.41

© ASCE

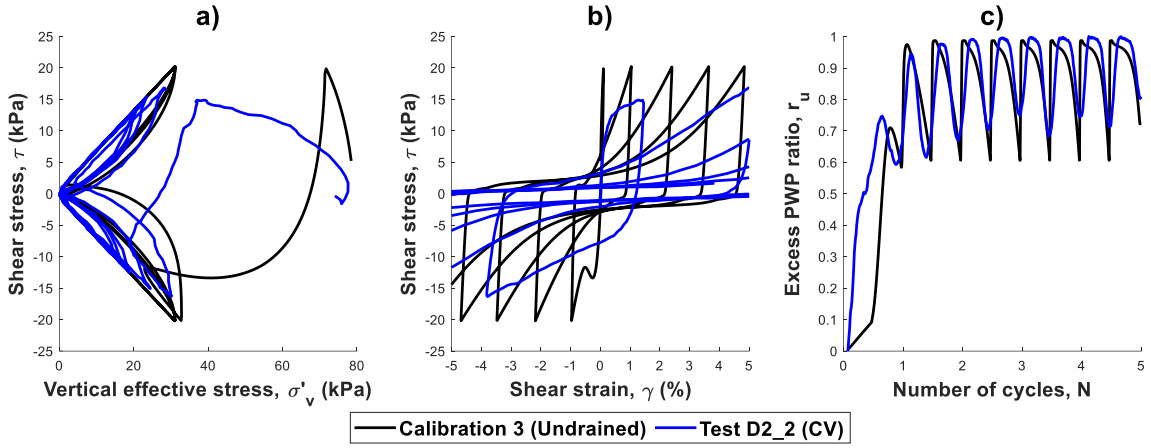


Figure 7. TU-calibrated simulations of CV cyclic loading response (Test D2_2, D_r 55%, CSR 0.26, σ'_{v0} = 79 kPa). a) Stress path, b) Stress-strain curve, c) PWP generation.

DISCUSSION

Simulated vs. experimental liquefaction triggering

From the biases in Table 5, the CV-calibrated models tended to underpredict liquefaction capacity measured from TU tests, which is consistent with Finn and Vaid's (1977) observations on Ottawa sand. The TU-calibrated model both over- and underpredicted liquefaction capacity measured from CV tests. Given the limited number of comparisons and small cycle counts lending to perception of significant errors, it is difficult to conclude from predicted N_f alone whether this is due to CV vs. TU calibrations. More experimental data is needed for further calibrations and cross-comparisons with simulations to conduct a more robust statistical assessment of bias.

Simulated vs. experimental cyclic responses

Figure 5 presents the cyclic response predicted by CV calibrations compared to the experimental TU cyclic response. The simulations generally provide good visual fit with the experimental response; the slopes of the critical state lines match, along with timing of peaks in excess PWP. From Figure 5c, Calibration 2 better matches the early-stage stress-path, and almost exactly matches the early rate of PWP generation with an early-stage mean error of -0.01. However, Calibration 1 better predicts overall PWP generation, with an overall mean error of 0.01 (Table 6) and ultimately has slightly less prediction error in N_f. From these results, there does not appear to be a clear advantage to calibrating to a capacity curve vs. a single test, even in the highly sensitive region of the liquefaction capacity curve.

Figures 6 and 7 present the cyclic response predicted by a TU-calibrated model compared to two experimental CV cyclic responses. Like in the CV calibrations, the simulations also provide good fits with the experimental responses in terms of location of critical state and timing of PWP peaks. Between the two CV predictions, the most significant differences are in the PWP generation, which was significantly better predicted for D2_2 (Figure 7c) compared to D1_4 (Figure 6c), with overall mean errors of 0.02 and -0.21, respectively (Table 6). This could be due

© ASCE

Downloaded from ascelibrary.org by California State University, Los Angeles on 03/07/25. Copyright ASCE. For personal use only; all rights reserved.

Downloaded from ascelibrary.org by California State University, Los Angeles on 03/07/25. Copyright ASCE. For personal use only; all rights reserved.

to the nature of the single test calibration not being able to capture overburden effects and lower CSR, as D1_4 was performed at σ'_{v0}=200 kPa and CSR=0.21 compared to the model calibrated to D2_2 at 72 kPa and CSR=0.31. D1_4's testing conditions lend to a denser soil fabric that could explain the smaller later-stage PWP peaks, due to less tendency for contractive behavior.

In comparing the CV vs. TU calibrations, the cyclic responses provide insight that the N_f predictions alone cannot capture. Disregarding Calibration 1 and considering only single test calibrations, differences arise in the modelled early-stage PWP generation. As seen in Figures 6c and 7c, the TU calibration tended to predict slower rates of PWP generation than the CV experiments for $N < 0.5$ (mean errors of 0.18 and 0.41), while from Figure 5c the CV calibration matched the experimental TU response exactly (mean error of -0.01). This could be due to the realities of TU testing, especially on loose coarse sands, where it can be difficult to retain PWP during shearing under a constant vertical load, resulting in dissipation of PWP, slower reduction of effective stresses, and therefore higher perceived liquefaction capacity. In comparison, height control in CV testing is better standardized and implemented in strict tolerances, resulting in less error in measured PWP generation, less perceived PWP dissipation, and lower perceived liquefaction capacity. The implications for constitutive model calibration are that TU-calibrated models may tend to overpredict CV tests, and CV-calibrated models may tend to underpredict TU tests, due to different implementations of the undrained condition during experimental testing.

CONCLUSION

This paper evaluated the performance of PM4Sand models calibrated to CV- and TU- cyclic DSS tests on medium-dense samples of Ottawa sand with relative densities ranging from 50-69% and CSR ranging from 0.125-0.31. For these conditions, CV-calibrated models tended to underpredict liquefaction capacity measured from a TU test, and the TU-calibrated model tended to predict slower early-stage rates of PWP generation than measured in CV tests. These differences could arise from the different ways that the undrained condition is experimentally implemented. Although consensus has been that PWP responses from CV and TU tests are equivalent for practical purposes, under marginal or extreme loading conditions, even small differences in the calibrated PWP response can significantly affect liquefaction predictions, as liquefaction is highly sensitive to PWP buildup. Further work following a similar framework of cross-comparisons could be conducted on a larger dataset considering a wider range of relative densities and CSR to quantify potential differences between CV- and TU-calibrated models across contractive and dilatant behaviors. Of particular interest would be conditions with high CSR and exhibiting low N_f, where it is critical yet more difficult to constrain predicted liquefaction behavior. Such a framework could also be used to evaluate the effects of CV- vs. TU-calibrated models for constitutive models other than PM4Sand. Finally, bender elements could be installed in the existing experimental setup to measure shear wave velocity and further constrain G_o. Overall, this study highlights the importance of understanding the experimental contexts behind inputs into numerical models.

ACKNOWLEDGEMENT

The National Science Foundation, with Award No. # 2117908, supported acquiring the CMDSS device. This work has also been partially supported by the National Science Foundation

© ASCE

with Award No. HRD-2112554. Cesar Leal is a recipient of the CREST-CATSUS fellowship, for which we are grateful. These supports are gratefully acknowledged.

REFERENCES

Anthi, M., and Gerolymos, N. (2019). "A Calibration Procedure for Sand Plasticity Modeling in Earthquake Engineering: Application to TA-GER, UBCSAND and PM4SAND." *7th International Conference on Earthquake Geotechnical Engineering*, Roma, Italy.

Andrus, R. D., and Stokoe, K. H., II. (2000). "Liquefaction resistance of soils from shear wave velocity", *J. Geotech. Geoenviron. Eng.*, ASCE, 126 (11), 1015–1025.

ASTM. (2019). D8296-19: *Standard test method for consolidated undrained cyclic direct simple shear test under constant volume with load control or displacement control*. American Society for Testing Materials.

Boulanger, R. W., and Ziotopoulou, K. (2017). *Plasticity Model for Sand (PM4Sand) Version 3.1*. University of California at Davis.

Dyvik, R., Berre, T., Lacasse, S., and Raadim, B. (1987). "Comparison of truly undrained and constant volume direct simple shear tests." *Geotechnique*, 37(1), 3-10.

El Ghoraiby, M. A., Park, H., and Manzari, M. T. (2017). *LEAP 2017: Soil Characterization and Element Tests for Ottawa F-65 Sand*. Department of Civil and Environmental Engineering, The George Washington University.

Finn, W. D. L., and Vaid, Y. P. (1977). "Liquefaction potential from drained constant volume cyclic simple shear tests." *Proc. 6th World Conf. Earthquake Engineering*, New Delhi 6, 7-12.

Hanley, K. J., Huang, X., O'Sullivan, C., and Kwok, F. (2013). "Challenges of Simulating Undrained Tests Using the Constant Volume Method in DEM." *AIP Conf. Proc.* 1542, 277–280.

Idriss, I. M., and Boulanger, R. W. (2008). Soil liquefaction during earthquakes. Monograph MNO-12, Earthquake Engineering Research Institute, Oakland, CA, pp. 261.

Itasca. (2016). *FLAC – Fast Lagrangian Analysis of Continua, Version 8.0*, Itasca Consulting Group, Inc., Minneapolis, MN.

Kwan, W. S., Leal, C., Nunez, E., and De Jesus, B. (2025). Partially Drained Responses of Dense Sand under Monotonic Simple Shear. *Geotechnical Frontiers 2025*. (paper submitted).

Lingwall, B. N. (2017). "Calibration of the PM4Sand Model for Sands with Substantial Amounts of Fines." *Geotechnical Frontiers 2017*, 321–31.

Luna, L. M. C., Lee, M., deJager, M., DeJong, J. T., Gomez, M. G., and Ziotopoulou, K. (2024). "A Liquefaction Triggering Surface for Ottawa F65 Sand: Cyclic DSS Results and PM4Sand Calibration." *Geo-Congress 2024*, 330–40.

MathWorks. (2024). *Curve Fitting Toolbox, MATLAB Version R2024a*. The MathWorks Inc., Natick, MA.

Youd, T. L., Idriss, I. M., Andrus, R. D., Arango, I., Castro, G., and Christian, J. T. (2001). "Liquefaction resistance of soils: Summary report from the 1996 NCEER and NCEER/NSF workshops on evaluation of liquefaction resistance of soils." *Journal of Geotechnical and Geoenvironmental Engineering*, ASCE 2001.127: 817–833.

Downloaded from ascelibrary.org by California State University, Los Angeles on 03/07/25. Copyright ASCE. For personal use only; all rights reserved.

© ASCE

Zhang, W., and Rothenburg, L. (2020). “Comparison of Undrained Behaviors of Granular Media Using Fluid-Coupled Discrete Element Method and Constant Volume Method.” *Journal of Rock Mechanics and Geotechnical Engineering* 12, no. 6 (December 2020): 1272–89.

Ziotopoulou, K., Montgomery, J., Bastidas, A. M. P., and Morales, B. (2018). “Cyclic Strength of Ottawa F-65 Sand: Laboratory Testing and Constitutive Model Calibration.” *Geotechnical Earthquake Engineering and Soil Dynamics V*, 180–89.

Downloaded from ascelibrary.org by California State University, Los Angeles on 03/07/25. Copyright ASCE. For personal use only; all rights reserved.

© ASCE